Korean J. Chem. Eng., **28**(8), 1764-1769 (2011)
DOI: 10.1007/s11814-011-0033-5

$Ce_{0.9}Sr_{0.1}Cr_{0.5}Mn_{0.5}O_{3-\delta}$ as the anode materials for solid oxide fuel cells running on H_2 and H_2S

Xiufang Zhu*, Han Yan*, Qin Zhong*,†, Xuejun Zhao*, and Wenyi Tan**

*School of Chemical Engineering, Nanjing University of Science and Technology, Nanjing 210094, P. R. China
**Department of Environment Engineering, Nanjing Institute of Technology, Nanjing 211167, P. R. China
(*Received 10 December 2010 • accepted 12 February 2011*)

Abstract−Perovskite-type $Ce_{0.9}Sr_{0.1}Cr_{0.5}Mn_{0.5}O_{3-\delta}$ (CSCMn) was synthesized and evaluated as anode for solid oxygen fuel cells based on $Ce_{0.8}Sm_{0.2}O_{1.9}$ (SDC). The conductivities of CSCMn were evaluated with DC four-probe method in 3% H_2-N_2 and 5% H_2S-N_2 at 450-700 °C, respectively. The compositions of CSCMn powders were studied by XRD and thermodynamic calculations. Meanwhile, sintering temperatures affecting phases of CSCMn is also proposed with XRD, and the analysis is given with thermodynamic calculations. CSCMn exhibits good chemical compatibility with electrolyte (SDC) in N_2. After exposure to 5% H_2S-N_2 for 5 h at 800 °C, CSCMn crystal structures change and some sulfides are detected, as evidenced by XRD and Raman analyses. The electrochemical properties are measured for the cell comprising CSCMn- SDC/SDC/Ag in 5% H_2S-N_2 at 600 °C and in 3% H_2-N_2 at 450 and 500 °C. The electrochemical impedance spectrum (EIS) is used to analyze ohm and polarization resistance of the cell at various temperatures.

Key words: Solid Oxygen Fuel Cell, Hydrogen Sulfide, Hydrogen, Anode Catalyst, Electrical Conductivity

INTRODUCTION

Solid oxide fuel cells (SOFCs) are an attractive energy conversion device for high fuel conversion efficiency; low emissions, low noise, renewable energy [1-7] and fuel flexibility are the biggest advantages for SOFCs. Most fuels are coal gas, biogas, and nature gas even industrial H_2 containing impurities such as S and P [8]. However, sulfur is a well-known poison for nickel catalysts [9,10]; sulfur chemisorbs on nickel, which blocks active nickel sites and leads to rapid performance degradation [8,11]. The poisoning effect of sulfur on the electrochemical performance of SOFCs has been the subject of numerous studies, where it is often reported to be reversible and the degradation speed related to operating temperature and H_2S concentration [12-17]. It leads to an almost activation polarization loss increasing very fast when sulfur is present in the fuel gas. For instance in [17], 0.5 ppm of H_2S at 100 mA/cm^2 current densities was reported to cause an almost 20% polarization loss.

In 2009, Jingli Luo et al. studied the performance of $Ce_{0.9}Sr_{0.1}VO_{3-\delta}$ (CSV) [18] and $Ce_{0.9}Sr_{0.1}Cr_{0.5}V_{0.5}O_{3-\delta}$ (CSCV) [19] in H_2S and H_2. They found that the catalyst activity of CSCV and CSV was much higher in H_2S than that of in H_2, even though some CSCV and CSV reacted with H_2S to generate $Ce_{0.9}Sr_{0.1}Cr_{0.5}V_{0.5}(O,S)_{3-\delta}$ and $Ce_{0.9}Sr_{0.1}V(S,O)_{3-\delta}$. These materials still are promising anode for SOFC for the higher conductivity and performance of the cell. But for the V-based compounds which are poisonous to health and have a higher price, it is crucial to find some low toxicity and cheaper transitional metals replacing the V-based.

In this work, Mn-based compounds as multivalent transition metal are utilized to be substitute for V-based compounds. The properties of $Ce_{0.9}Sr_{0.1}Cr_{0.5}Mn_{0.5}O_{3-\delta}$ as anode are investigated in 5% H_2S and 3% H_2 below 700 °C, respectively. The chemical stability, electrical conductivity, thermodynamic calculations and electrochemical activity are discussed under conditions relating to SOFCs. The electrochemical impedance spectrum (EIS) is used to analyze the impact of R_p and R_o on the performance of the cells.

†To whom correspondence should be addressed.
E-mail: xiufangzhu@163.com

EXPERIMENT

1. Preparation of Anode Materials

$Ce_{0.9}Sr_{0.1}Cr_{0.5}Mn_{0.5}O_{3-\delta}$ (CSCMn) powders were synthesized by gel combustion method [18,19]. Simply, stoichiometric $Ce(NO_3)_3{\cdot}6H_2O$, $Sr(NO_3)_2$, $Cr(NO_3)_3{\cdot}9H_2O$ and $Mn(CH_3COO)_2{\cdot}4H_2O$ were weighed and dissolved in distilled water. A certain amount of citric acid was added with stirring and ammonium hydroxide was applied to adjust the pH to ~7. Under stirring and heating at 80 °C, a viscous gray gel was obtained, which was heated continually at 100 °C until combusted to get porous ash. The ash was reduced in 3% H_2-N_2 at 1,100 °C for 5 h.

2. Electrolyte and Cathode

$Ce_{0.8}Sm_{0.2}O_{1.9}$ (SDC) powders as the electrolyte were prepared by EDTA-citric complexing method [20]. Sm_2O_3 pre-dissolved in HNO_3 and $Ce(NO_3)_3{\cdot}6H_2O$ were dissolved at the stoichiometric ratio. A certain amount of EDTA-$NH_3{\cdot}H_2O$ and citric acid as complexing agent was added with stirring. Ammonia was used to adjust the pH to ~10. The solution was heated with stirring at above 90 °C to get a yellow transparent gel. And then the gel was baked in 180 °C for 18 h. The powders were calcined at 900 °C for 6 h in air, and then the powders were pressed into a pellet; the pellet's thickness was 0.5 mm and its diameter 12 mm. The wafer was sintered at 1,100 °C for 4 h as support.

The cathode material was silver epoxy adhesive (CB-813, CRC-BonD Co, LTD). The cathode with the thickness of 50 μm adhered to electrolyte by the screen printing method. Then the sample was

fired in N_2 at 800 °C for 4 h to achieve densification, as shown in Fig. 1 [21].

3. Characterization and Electrochemical Test

The phase identification of CSCMn was characterized by X-ray diffraction (XRD Bruker D8 ADVANCE, Germany) with Cu Kα radiation in the 2θ range from 20° to 80°. Thermodynamic calculations were performed using HSC Chemistry®5.0 to generate phase diagrams of the ternary component systems [22,23]. The morphologies of synthesized powders and the cross-section of the cell were determined using a scanning electron microscope (Flexscan L367 S-3000N, HITACHI). The conductivities of CSCMn in 5% H_2S and 3% H_2 were measured by four-probe method for the symmetrical cell with the configuration of Ag/CSCMn/Ag, respectively, and the electrochemical test of fuel cell was recorded via electrochemical station (CHI 660D, Chen hua, Shanghai). The range of the frequency was from 0.1 Hz to 10^6 Hz.

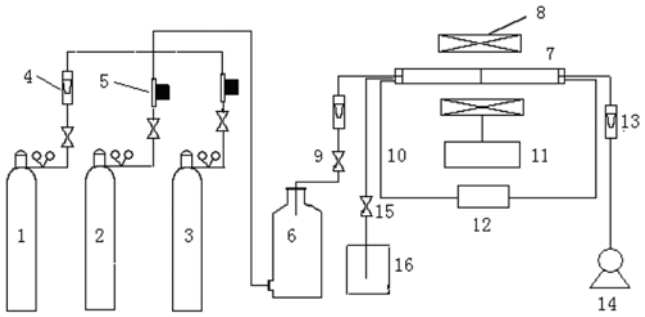

Fig. 1. Schematic diagram of experimental apparatus for sulfur-tolerant anode test.

1. H_2S+N_2 gas cylinder
2. H_2 gas cylinder
3. N_2 gas cylinder
4. Rotameter
5. Mass flow meter
6. Bbuffered bottle
7. Reacter of SOFC
8. Furnace
9. Intake port collection
10. Ag line
11. Temperature controller
12. CHI660D electrochemical workstation
13. Air rotameter
14. Air compressor
15. Outtake port collection
16. Off-gas absorption container

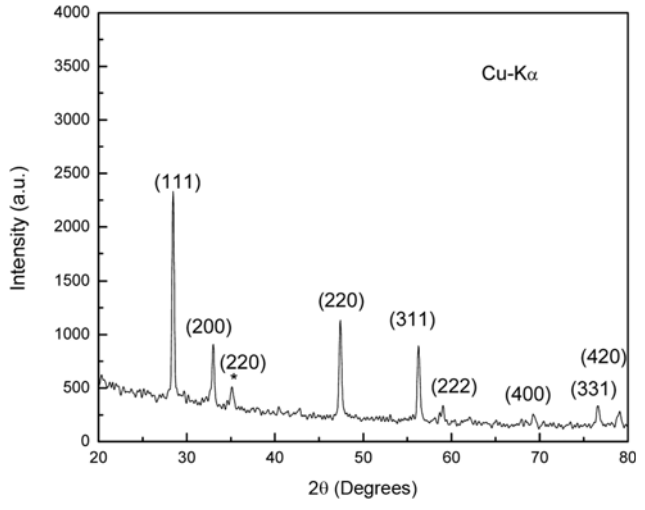

Fig. 2. XRD pattern of CSCMn powders after reduction in 3% H_2-N_2 at 1,100 °C for 5 h (* standing for CeO (200)).

RESULTS AND DISCUSSION

1. XRD of Precursor Powders

The XRD pattern of the $Ce_{0.9}Sr_{0.1}Cr_{0.5}Mn_{0.5}O_{3-\delta}$ powders (Fig. 2)

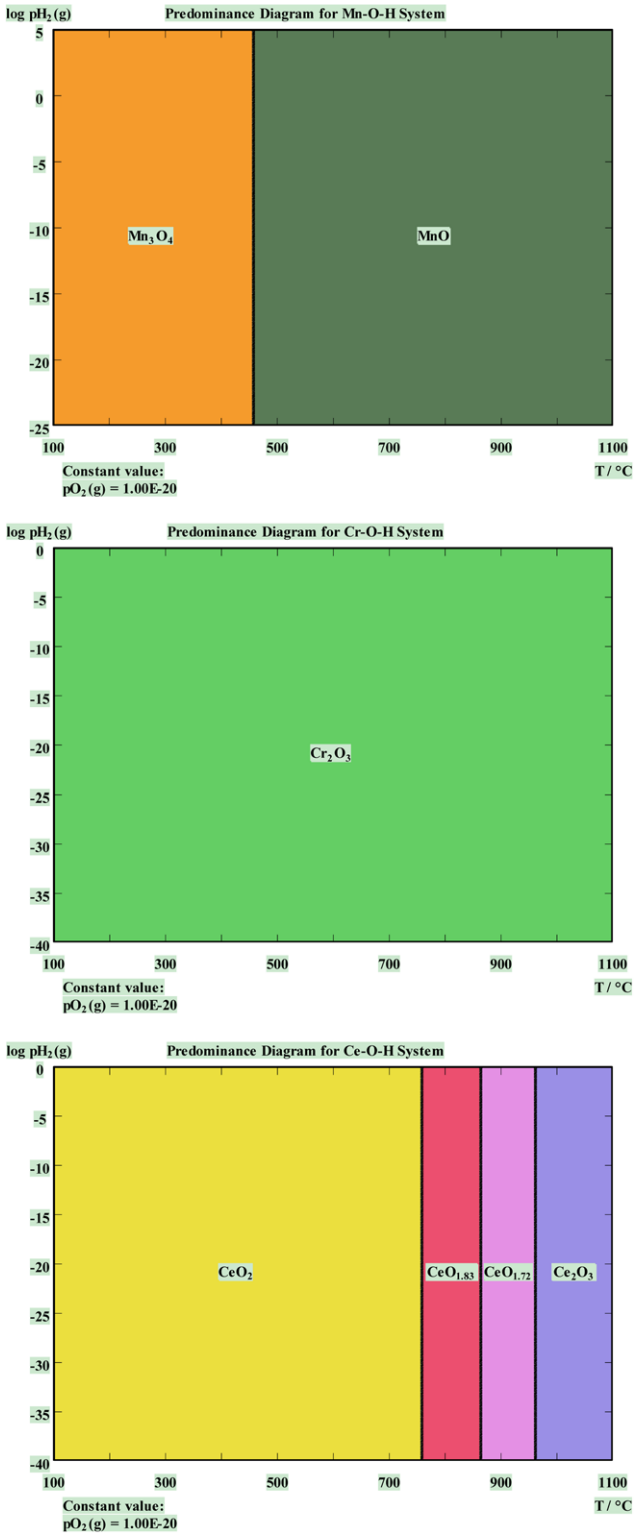

Fig. 3. Phase equilibrium of the Mn-O-H, Ce-O-H and Cr-O-H system at various temperatures derives from HSC Chemistry.

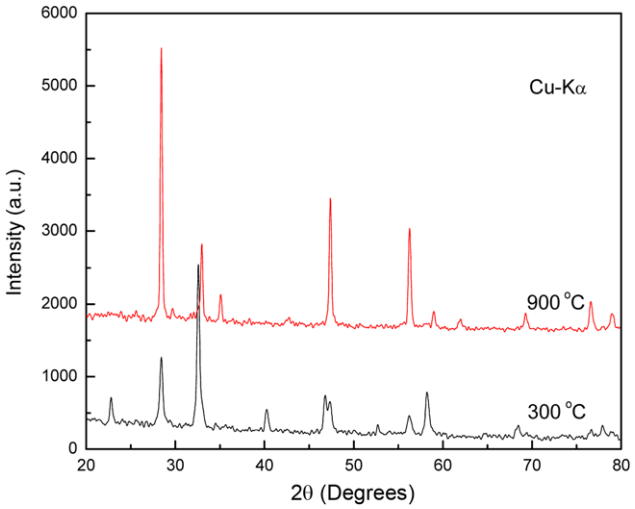

Fig. 4. XRD pattern of CSCMn powders in air at 300 and 900 °C for 4 h.

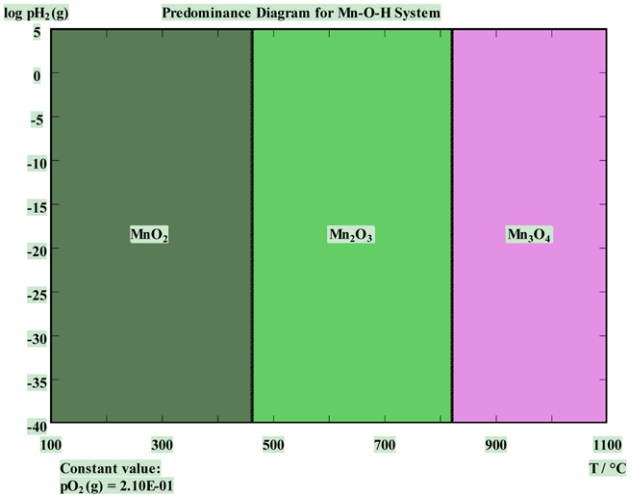

Fig. 5. Phase equilibrium of the Mn-H-O system at various temperatures in air sintering.

shows that the phase formations of the powder samples possess perovskite structures with the following lattice parameters: cell volume: v=159.5 Å^3 and the parameter: a=5.424 Å, which is similar to that of the CeO_2 parent (JCPDS card No. 81-0792). The thermodynamic calculation (Fig. 3) indicates that Ce, Cr and Mn oxides existed in the reduction state in 3% H_2 at 1,100 °C. Sr was found to be far more resistant to reaction with sulfur than Ce, and due to its low (10 mol% in ceria) concentration in CSCMn; Sr was not considered further in this study [22]. Fig. 4 illustrates the temperature affects the crystal structure of CSCMn. The reason can be found from the thermodynamic calculation (Fig. 5). Fig. 5 indicates that MnO_2 is the main phase below 450 °C; Mn_3O_4 dominates beyond 810 °C, while Mn_2O_3 is primary product at interval temperatures. The result explains the XRD difference of CSCMn at 300 and 900 °C. The average crystallite size calculated is 10-40 nm from Scherrer's formula as Eq. (1).

$$D=K\lambda/\beta\cos\theta \quad (1)$$

Where D is the particle size, K is the Scherrer constant, λ is the

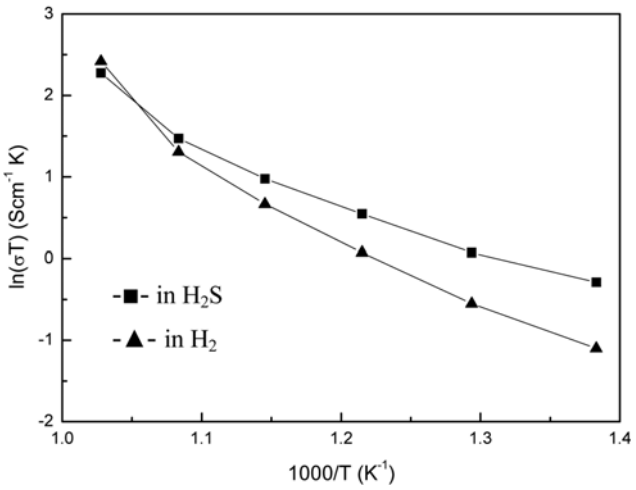

Fig. 6. Conductivities of CSCMn in 5% H_2S-N_2 and 3% H_2-N_2 at various temperatures.

X-ray radiation wavelength, θ is the angle of XRD peak, and β is the full width at half maxima (FWHM). After correction the formula is as follows (2):

$$D=\frac{0.89\times0.15406}{\frac{(\beta-0.09)}{180}\times\pi\times\cos\theta} \quad (2)$$

2. Conductivity Testing

The conductivities of CSCMn were investigated in 5% H_2S-N_2 and 3% H_2-N_2. From Fig. 6 we can see that they increase with the temperature elevated, and the properties are similar to that of semiconductors and ionic conductors [24]. The almost linear relationship between ln(σT) and 1/T indicates that the conductivit behavior is a thermally activated process associated with a temperature-independent carrier concentration [25] that obeys the small polaron conductivity mechanism expressed in the following equation:

$$\sigma=\left(\frac{A}{T}\right)\exp\left(\frac{-E_a}{kT}\right) \quad (3)$$

where A is the pre-exponential factor, k is Boltzmann's constant, T is the absolute temperature and E_a is the activation energy. The electrical conductivities are 5.1 S/cm in H_2S and 4.9 S/cm in H_2 at 700 °C, respectively. The results indicate that CSCMn catalyzed activities in H_2S are superior to H_2. From the activation energy values, the same conclusion can be drawn. The activation energies calculated from the Arrhenius equation are 0.81 eV and 0.61 eV in 3% H_2 and 5% H_2S, correspondingly. The reason maybe is that the CSCMn occurs reforming in H_2S forming Ce-O-S phases, which is consistent with Ref. [18,19].

For the perovskite oxide, the electrical conductivity goes hand in hand with the phase structures and the characters of the mutable metal ions at the B-site. The electron conduction in perovskite is created by B-site lattice cations through strongly overlapping B^{n+}-O^{2-}-$B^{(n+1)+}$ bonds and the mechanism maybe like the Zerner double exchange process which is shown as the following:

$$B^{n+}-O^{2-}-B^{(n+1)+}\Rightarrow B^{(n+1)+}-O^{-}-B^{(n+1)+}\Rightarrow B^{(n+1)+}-O^{2-}-B^{n+}$$

Due to the variable metal at B-site, it is possible for the electron

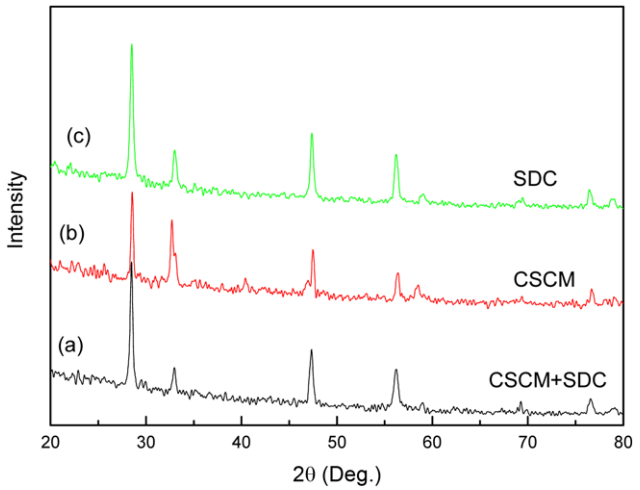

Fig. 7. XRD patterns of CSCMn, SDC and the mixture of them after calcined at 900 °C for 2 h in N_2.

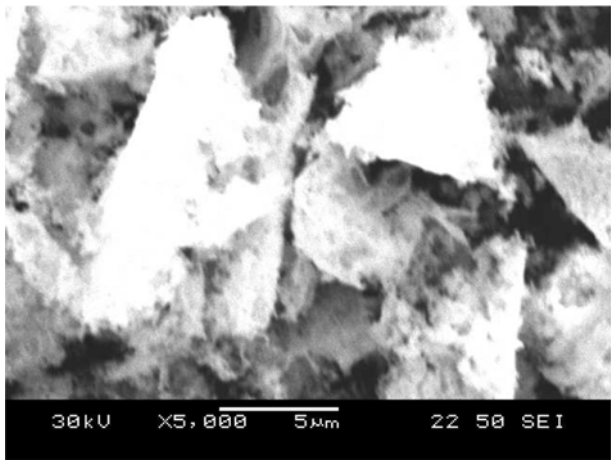

Fig. 9. SEM micrograph of CSCMn after calcined at 1,100 °C for 5 h in 3% H_2-N_2.

conduction through the overlapping of 2p of oxygen with the 3d orbital of Cr and Mn [26]. The main reason will be studied in future work.

3. Chemical Stability and Powder Morphology

Comparing the XRD patterns of CSCMn, SDC and the disc of CSCMn+SDC (rate of mass is 1 : 1) mixture after calcination at 900 °C for 2 h in N_2, as shown in Fig. 7, it is clear that CSCMn has a good chemical compatibility with electrolyte SDC in N_2, and no other new phases are detected. The result shows $Ce_{0.9}Sr_{0.1}Cr_{0.5}Mn_{0.5}O_{3-\delta}$ is suitable to be used as the anode materials of electrolyte SDC. By comparing the XRD and Raman of before and after exposure to H_2S for 5 h at 800 °C, some changes of CSCMn crystal structure have happened as illustrated in Fig. 8. The reason may be that some Ce-O-S phases are formed in higher concentration H_2S. The result is consistent with CSCV. An intense Raman band around 465 cm^{-1} is the Raman spectra of CeO_2; fluorite structure-metal dioxides have only a single allowed Raman mode, which has F_{2g} symmetry and can be viewed as a symmetric breathing mode of the O atoms around each cation [27-30].

Fig. 9 reveals the SEM micrographs of CSCMn after calcining at 1,100 °C for 5 h in 3% H_2-N_2. CSCMn is a sheet structure and catalyst particles are well dispersed and the structure has good porosity.

4. Fuel Cell Testing

Fuel cell test is carried out to determine the electrochemical activity of the anode material for conversion of H_2S and H_2, Fig. 10 presents the I-V and I-P curves for CSCMn-SDC/SDC/Ag in 5% H_2S-N_2 at 600 °C, Fig. 11 gives the I-V and I-P curves in 3% H_2-N_2 at 450 °C and 500 °C, respectively. The max open circuit voltages are 0.87 V at 600 °C in 5% H_2S-N_2 and 0.91 V at 500 °C in 3% H_2-N_2. The max power densities are 6.56 mW/cm^2 and 8.18 mW/cm^2, correspondingly. The linear behavior of the I-V curve is probably due to the thickness of electrolyte that hinders the activation of the CSCMn electrode, so Ohm polarization is the main reason affecting the battery. The conclusion agrees with the analysis of EIS. The EIS of CSCMn oxide was obtained at 450 °C and 500 °C in 3% H_2 as given in Fig. 12. Fig. 13 illustrates the equivalent circuit of the cell. The impedance spectra consisted of two semi-circles. This means that there are at least two electrode processes corresponding to the two

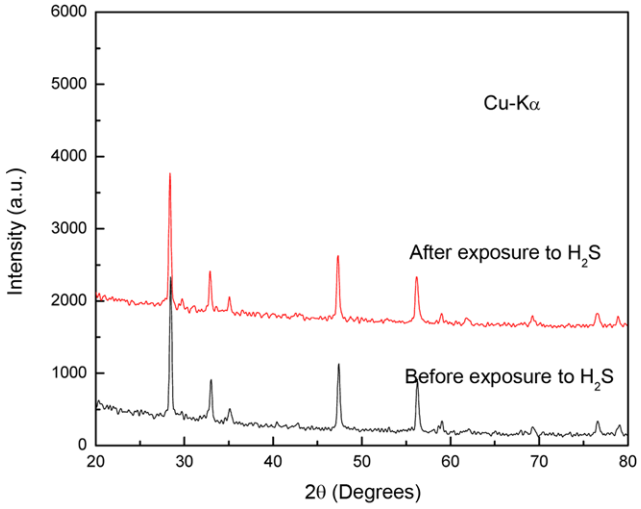

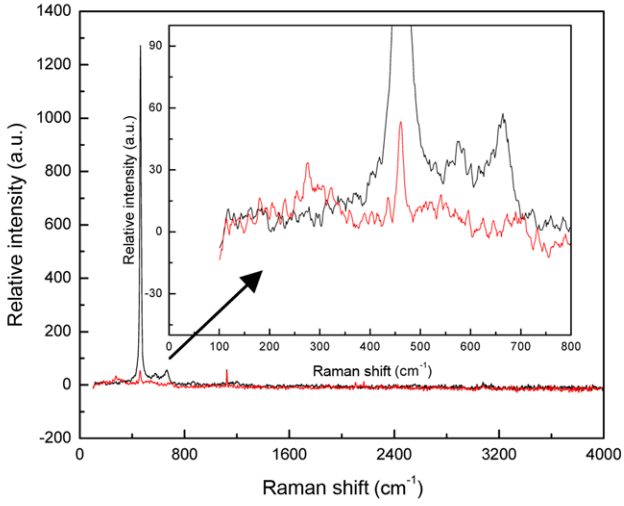

Fig. 8. XRD patterns and Raman spectrums of CSCMn before and after exposure to 5% H_2S for 5 h at 800 °C.

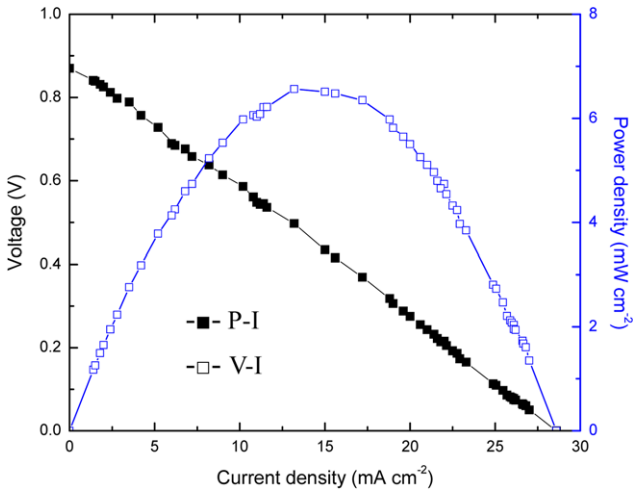

Fig. 10. I-V and P-I curves of single cell with CSCMn-SDC|SDC|Ag in 5% H_2S-N_2 at 600 °C.

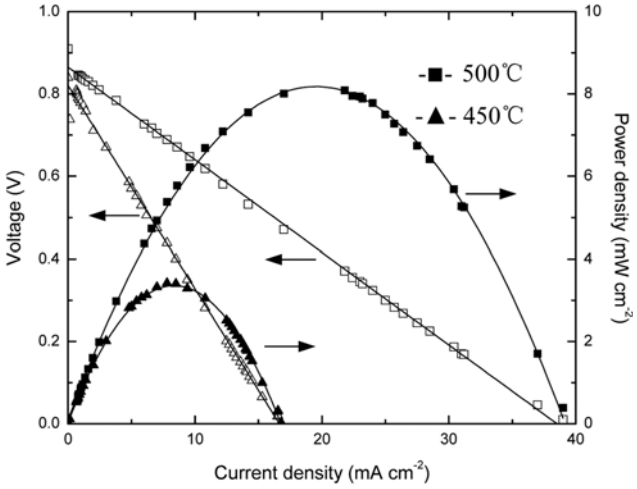

Fig. 11. I-V and I-P curves of single cell with CSCMn-SDC|SDC|Ag in 3% H_2-N_2 at 450 and 500 °C.

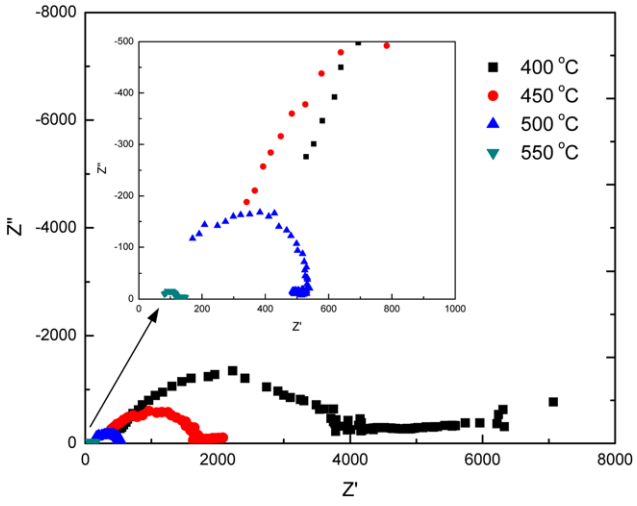

Fig. 12. EIS of CSCMn electrode in 3% H_2 at various temperatures.

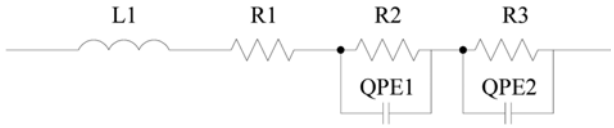

Fig. 13. Equivalent circuit model of EIS at 550 °C.

semi-circles during molecular hydrogen oxidation. According to references [31,32], the semi-circle at the high frequency can be considered the polarization during the process of charge transfer. On the other hand, the semi-circle at the low frequency can be considered to be anode gas adsorption/dissociation and bulk or surface hydrogen diffusion process. Therefore, in the equivalent circuit, L1 is an inductance induced by the cables; R1 stands for the Ohmic resistance including the electrolyte resistance and lead wires [33]. R2 is represented as the resistance of the charge transfer process through the electrode-electrolyte interface; R3 is referred to as the resistance of the anode gas (hydrogen) adsorption/desorption and bulk or surface diffusion process; QPE1 and QPE2 correspond to the capacitance of the whole electrode. Obviously, the area specific resistance significantly decreases with the increasing temperature as shown in Fig. 12.

CONCLUSIONS

Anode powders CSCMn were prepared by gel combustion method. The conductivities of catalyst measured were 5.1 S/cm in H_2S and 4.9 S/cm in H_2 at 700 °C, respectively. The structure was evaluated by XRD and thermodynamic calculation. CSCMn powders exhibit good chemical compatibility with the electrolyte (SDC) in N_2. However, the stability in H_2S reductive atmosphere is poor through XRD and Raman analysis. The result is consistent with $Ce_{0.9}Sr_{0.1}VO_{3-\delta}$ and $Ce_{0.9}Sr_{0.1}Cr_{0.5}V_{0.5}O_{3-\delta}$. The characteristics of the cells with configuration of CSCMn-SDC/SDC/Ag are measured in different atmosphere. The open circuit voltages are 0.87 V at 600 °C in 5% H_2S-N_2 and 0.91 V at 500 °C in 3% H_2-N_2, the maximal power densities are 6.56 mW/cm^2 and 8.18 mW/cm^2. After EIS analysis, the area specific resistance significantly decreases with the increasing temperature.

ACKNOWLEDGEMENTS

The work was supported by the Funds of Nature Science of Jiangsu Province (Grant No. BF2006208 and No. BK2010478).

REFERENCES

1. G. Meng, G. Ma, R. Peng and X. L.iu, *Solide State Ionics*, **178**, 697 (2007).
2. M. C. Williams, B. R. Utz and K. M. Moore, *J. Fuel Cell Sci. Technol.*, **1**, 81 (2004).
3. H. Kurokawa, L. Yang, C. P. Jacobson, L. C. De Jonghe and S. J. J. Visco, *J. Power Sources*, **164**, 510 (2007).
4. F. Baratto, M. Urmila and Diwekar, *J. Power Sources*, **139**, 188 (2005).
5. C. S. Song, *Catal. Today*, **77**, 17 (2002).
6. Z. P. Shao and S. M. Haile, *Nature*, **431**, 170 (2004).

7. T. Norby, *Solid State Ion.,* **125**, 1 (1999).
8. Xiufu Sun, 8th SERC Biannual Meeting (2010).
9. F. P. Nagel, T. J. Schildhauer, J. Sfeir, A. Schuler and S. M. A. Biollaz, *J. Power Sources*, **189**, 1127 (2009).
10. M. V. Twigg, *Catalyst Handbook*, Wolfe Publishing Ltd., Frome, England (1989).
11. U. Hennings, M. Brune and R. Reimert, *GWF Gas Erdas*, **145**, 92 (2004).
12. O. Marina, L. R. Pederson, D. J. Edwards, C. W. Coyle, J. Templeton, M. Engelhard and Z. Zhu, *Arsenic and sulfur impurities*, in: Proceedings of the 8th Annual SECA Workshop, San Antonio, United States of America (2007).
13. R. H. Cunningham, M.Fowles, R.M. Ormerod, J. Staniforth, *DTI*, Report F/01/00222/REP (2004).
14. N. Arnstein, *Experimental investigation of solid oxide fuel cells using biomass gasification producer gases*, Norwegian University of Science and Technology, Trondheim, Norway (2005).
15. L. Aguilar, S. Zha, Z. Cheng, J. Winnick and M. Liu, *J. Power Sources*, **135**, 17 (2004).
16. Y. Matsuzaki and Y. Isamu, *Solid State Ionics*, **132**, 261 (2000).
17. E. Brightman, D. G. Ivey, D. J. L. Brett and N. P. Brandon, *J. Power Sources*, In press.
18. N. Danilovic, J. L. Luo, K. T. Chuang and A. R. Sanger, *J. Power Sources*, **194**, 252 (2009).
19. N. Danilovic, J. L. Luo, K. T. Chuang and A. R. Sanger, *J. Power Sources*, **192**, 247 (2009).
20. W. C. Wu, J. T. Huang and A. Chiba, *J. Power Sources*, **195**, 5868 (2010).
21. X. F. Zhu, Q. Zhong, X. J. Zhao and H. Yan, *Appl. Surf. Sci.*, **257**, 1967 (2011).
22. P. Lohsoontorn, D. J. L. Brett and N. P. Brandon, *J. Power Sources*, **175**, 60 (2008).
23. OUTOKUMPU, HSC Chemistry for Windows, Version 5.0, OUTOKUMPU.
24. C. Kittel, Introduction to Solid State Physics, 8th ed., Wiley, Berkley, CA (2005).
25. W. J. Weber, C. W. Griffin and L. Bates, *J. Am. Ceram. Soc*., **70**(4), 265 (1987).
26. H. X. Gu, Y. Zheng, R. Ran, Z. P. Shao, W. Q. Jin, N. Xu and J. Ahn, *J. Power Sources*, **183**, 471 (2008).
27. J. R. McBride, K. C. Hass, B. D. Poindexter and W. H. Weber, *J. Appl. Phys*., **76**, 2435 (1994).
28. M. Zunica, L. Chevallier, A. Radojkovic, G. Brankovic, Z. Brankovic and E. D. Bartolomeo, *J. Alloy. Compd.*, **509**, 1157 (2011).
29. J. M. Im, H. J. You, Y. S. Yoon and D. W. Shin, *Ceramics International*, **34**, 877 (2008).
30. E. C. C. Souza and E. N. S. Muccillo, *J. Alloy. Compd.*, **473**, 560 (2009).
31. F. H. Heuveln and H. J. M. Bouwmeester, *J. Electrochem. Soc*., **144**, 134 (1997).
32. Y. J. Leng, S. H. Chan, K. A. Khor and S. P. Jiang, *Int. J. Hydrog. Energy*, **29**, 1025 (2004).
33. S. Q. Lv, G. H. Long, Y. Ji, X. W. Meng, H. Y. Zhao and C. C. Sun, *J. Alloy. Compd.*, In press.